IN-VENTO 2014
XIII Conference of the Italian Association for Wind Engineering
22-25 June 2014, Genova, Italy

Implementation of the non-flutter design principle

Michael Styrk Andersen[1], Emrah Sahin[2], Benjamin Laustsen[2], Michael Lenius[2] and Jesper Røssel Læsø[2]

[1]Research Assistant, University of Southern Denmark, Faculty of Engineering
[2]Student, M.Sc. Eng., University of Southern Denmark, Faculty of Engineering
Corresponding author: Michael Styrk Andersen, mian@iti.sdu.dk

Abstract

The non-flutter design principle is introduced. Aerodynamically stable section model tests performed by three different research groups indicate, that flutter might be avoided if the torsional-to-vertical frequency ratio is kept below 1. A case study of a suspension bridge spanning 3.7 km with a torsional-to-vertical frequency ratio $\gamma_\omega = 0.89$ is presented. Using a multimodal flutter approach and bridge deck flutter derivatives equal to those of a thin airfoil, classical flutter was shown not to occur.

1 Introduction

The aim of building super long span bridges in the future is challenging the civil engineering community. After the catastrophic collapse of the first Tacoma Narrows in 1940, modern bridge decks are designed with increased torsional stiffness to prevent flutter and torsional divergence. The introduction of the closed box girder amplified the torsional stiffness, but an increase in span width increase the cable contribution of the stiffness compared to the bridge deck it self which tends to decrease the torsional-to-vertical frequency ratio.

The torsional-to-vertical frequency ratio, $\gamma_\omega = \frac{\omega_\alpha}{\omega_\xi}$ where ω_α and ω_ξ is the torsional and vertical natural frequencies respectively, are decisive for the critical flutter wind velocity. In traditional bridge design, this means that the required torsional stiffness of the bridge deck is increased when the span goes up, which means that the mass of the bridge deck per unit length is increased as well as the total costs, because that is roughly proportional to the mass of the bridge deck. Aerodynamic countermeasures against flutter increases the unit cost of the bridge deck as well.

Richardson (1981) demonstrated that the cost of required torsional stiffness of the bridge deck to prevent flutter, is exponential to the span of the bridge. Therefore he introduced the idea of a twin suspension bridge having a torsional-to-vertical frequency ratio below unity. Lateral cross beams were placed between the twin girders and the cable planes were located at the internal side of the girders.

The principle of decreasing the torsional frequency to the level of the vertical frequency or below has been labeled the non-flutter design principle (Dyrbye and Hansen, 1997; Johansson et al., 2013). Dyrbye and Hansen (1997) explained that for very long span suspension bridges, the torsional rigidity of a closed box girder is too small to resist flutter. In order to obtain large critical flutter wind velocities, they proposed a design in which the torsional and vertical frequencies deliberately were made identical. This concept was validated experimentally by Bartoli et al. (2009).

1.1 Experimental validation

Bartoli et al. (2009) made wind tunnel experiments with a modified Messina twin bridge section model where $\gamma_\omega = 1.00$ and proved that it was stable against flutter, which confirms the thesis of (Richardson, 1981) and (Dyrbye and Hansen, 1997).

Wind tunnel tests performed recently (Johansson et al., 2013) and (Nowicki and Flaga, 2011) reports that flutter does not occur for flat plate section models with torsional-to-vertical frequency ratios below

1. Nowicki and Flaga (2011) reported, however, that this was not the case for bluff body bridge deck sections. Torsional divergence was not reported.

The aerodynamic derivatives and structural damping may be decisive for the limits of γ_ω, where the non-flutter frequency bandwidth is distinguished.

From the wind tunnel tests on section models, with frequency ratios close to or below unity, reported in the literature, there are no general value of the torsional-to-vertical frequency ratio γ_ω applicable to all bridge decks, which guarantees stability against violent flutter, because this limit depends on the aerodynamic derivatives of the section model.

The section model tests, reported in the literature, that do not show any sign of aerodynamic instability is:

- A single flat plate section model with a height-to-width ratio $h : b = 1 : 10$ and $\gamma_\omega = [0.71, 0.88]$ (Johansson et al., 2013)
- A single flat plate section model with a height-to-width ratio $h : b = 1 : 22$ and $\gamma_\omega = [0.81, 0.92]$ (Nowicki and Flaga, 2011)
- A single flat plate section model with a height-to-width ratio $h : b = 1 : 22$ and $\gamma_\omega = 1.08$ with increased structural damping (Nowicki and Flaga, 2011)
- A modified Messina Bridge section model (Twin boxes with curved shapes) and $\gamma_\omega = 1.00$ (Bartoli et al., 2008)

In the above mentioned wind tunnel tests, decreasing torsional frequencies have been reported due to increasing mean wind velocity. The decrease in torsional frequency is believed to increase the frequency separation between torsional and vertical modes, and thus, at least for the above mentioned cross section shapes, prevents the onset of classical coupled flutter.

Adapting the Theodorsen thin airfoil flutter derivatives (Theodorsen, 1934), there are no critical flutter wind velocity below a certain threshold, at $\gamma_\omega \approx 1.1$ (Dyrbye and Hansen, 1997). But the aerodynamically stable results of (Bartoli et al., 2008; Nowicki and Flaga, 2011; Johansson et al., 2013) with section models having torsional-to-vertical frequency ratios in the range $0.71 \leq \gamma_\omega \leq 1.08$ indicates that further experiments are needed to clarify the influence of $\gamma_\omega \leq 1.1$ for real bridge deck flutter derivatives.

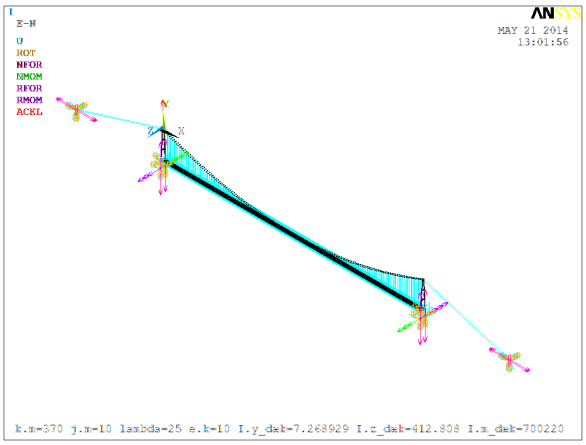

Figure 1. Finite element model used in a case study of a suspension bridge spanning 3.7 km. Various cross section properties are presented in Section 3, Table 2.

1.2 Present Study

In the present study, the aerodynamic coupling in classical bi-modal coupled flutter between pure vertical and torsional modes are investigated in section 2.1. The probability of classical bi-modal coupled flutter between all pure vertical and torsional modes are derived mathematically, eg. coupling between the second symmetric torsional mode with the first symmetric vertical mode. These results are verified in a case study of a suspension bridge design, illustrated in Figure 1, presented in Section 3.

It is, however, questionable whether flutter will occur between other modes than pure vertical and pure torsional modes. The presence of lateral torsional modes blurs the picture. In order to answer this question, a multimodal analysis with contributions of the first 20 bridge deck mode shapes is performed to reveal all possible flutter mechanisms in Section 3.3.

2 Probability of mode shape coupling

It is widely recognized that coupling of torsional and vertical mode shapes is considered to occur only between symmetric and antisymmetric pairs of mode shapes. But considering the structural mode shapes of the bridge deck as sine functions, it is seen that coupling is restricted only to occur between vertical and torsional mode shapes of the same order, due to the orthogonality of sine functions. An exception to this is coupling between the first and second symmetric mode shapes, which is described as the sum of two sines (Bleich et al., 1950). However, the product of the non dimensional mode shape coupling constants given in Equation (2) may become very close to zero.

The modes of a suspended bridge deck are strongly linked to the two main cable system modes. If the main cables oscillate in phase, pure vertical bending of the bridge deck will take place, while pure torsional oscillations of the bridge deck will take place when the main cables oscillate out of phase. (Bleich et al., 1950; Gimsing and Georgakis, 2012)

It is assumed that the mass and mass moment of inertia are uniformly distributed along the bridge deck axis. For super long span bridges the stiffness of the bridge deck itself is small compared to the stiffness provided by the cable suspension system. (Gimsing and Georgakis, 2012)

The vertical and torsional bridge deck mode shapes $\xi_n(y)$ and $\alpha_m(y)$ of the main span of a suspension bridge, has been described approximately by simple sine functions in the literature (Bleich et al., 1950), except the first and second symmetric modes, which can be described approximately as the sum of two sine functions. The former is considered below in Section 2.1 while the latter is treated in Section 2.2.

2.1 Mode coupling probability for antisymmetric and higher symmetric modes

The assumption of pure sine functions has been adapted in Equation (1) to show the tendency of mode coupling.

The bridge deck axis is denoted y. L is the main span width while n and m are the number of half-waves present in the respective mode shapes, where heave and pitch are denoted ξ and α respectively.

The natural frequencies ω_{ξ_n} and ω_{α_m} do not necessarily ascend according to the index n or m.

$$\xi_n(y) = \sin\frac{n\pi y}{L}, n \in N^+ \setminus \{1,3\} \tag{1a}$$

$$\alpha_m(y) = \sin\frac{m\pi y}{L}, m \in N^+ \setminus \{1,3\} \tag{1b}$$

The first 6 torsional and vertical mode shapes considered, are illustrated in Figure 2.

The similarity between mode shapes is described by the product of their mode shape coupling coefficients $c_{\xi,n}$ and $c_{\alpha,m}$ given in Equation (2). If the vertical bending mode shape $\xi_n(y)$ and the torsional mode shape $\alpha_m(y)$ has similar deflection curves along the bridge deck, the product $c_{\xi,n}c_{\alpha,m} = 1$. The bridge may be prone to classical flutter if $\frac{\omega_{\alpha m}}{\omega_{\xi_n}} > 1$, but if $c_{\xi,n}c_{\alpha,m} = 0$ coupled flutter does not arise.

$$c_{\xi_n} = \frac{\int_0^L \xi_n(y)\alpha_m(y)\,dy}{\int_0^L \xi_n^2(y)\,dy} \tag{2a}$$

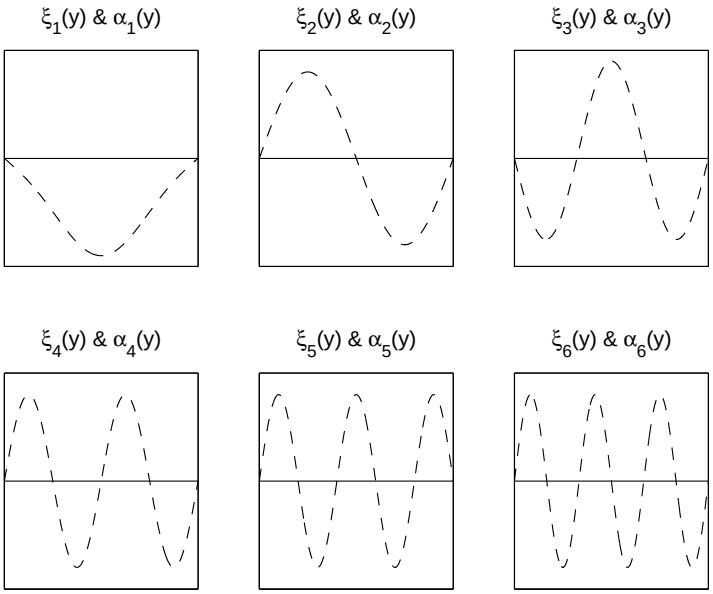

Figure 2. Vertical and torsional bridge deck mode shapes of the main span

$$c_{\alpha_m} = \frac{\int_0^L \xi_n(y)\alpha_m(y)\,dy}{\int_0^L \alpha_m^2(y)\,dy} \tag{2b}$$

The mode shape functions $\xi_n(y)$ and $\alpha_m(y)$ are mutually orthogonal on the interval $0 \leq y \leq L$. This means that the product of the mode shape coupling coefficients $c_{\xi,n}c_{\alpha,m} = 0$ if $n \neq m$, since

$$\int_0^L \sin\frac{n\pi y}{L}\sin\frac{m\pi y}{L}\,dy = \begin{cases} L/2 & \text{if } n = m \\ 0 & \text{otherwise} \end{cases} \tag{3}$$

2.2 Mode coupling probability for lower symmetric modes

For the first and second symmetric vertical and torsional mode shapes, where n and m equals 1 or 3, the curvature in Equation (4), along the bridge deck is defined as the sum of two sine terms.

$$\xi_n(y) = \sin\frac{\pi y}{L} + a_3\sin\frac{3\pi y}{L}, n = \{1,3\} \tag{4a}$$

$$\alpha_m(y) = \sin\frac{\pi y}{L} + a_3\sin\frac{3\pi y}{L}, m = \{1,3\} \tag{4b}$$

The coefficient a_3 depends on span width, side span width, girder stiffness, mass distribution and cable plane eccentricity.

The mode shape coupling coefficients between first ($n = 1$) symmetric vertical bending mode and second ($m = 3$) symmetric torsional mode must be analyzed in detail, because it is possible that $\gamma_\omega > 1$, even though the first symmetric vertical and torsional mode shape has $\gamma_\omega < 1$.

3 Case study: A concept for the Sognefjord Bridge

A twin suspension bridge with one central span of 3.7 km and a cable sag of 370 m has been modeled and analyzed with finite element software ANSYS Mechanical APDL, as illustrated in Figure 1.

The bridge deck is pinned to the pylons, but free at mid span. The cables are fixed at their ends and pinned to the top of the pylons. Three bracings connects the pylon legs 10, 130 and 250 meters from the

top level of the pylons. The pylon legs are fixed to the ground.

The cable cross sectional area has been estimated to withstand dead- and live load. The mechanical properties of the main cable and the hangers are given in (Gimsing and Georgakis, 2012). The total mass of the twin bridge cross section are $m = 14.57t/m$ while the mass moment of inertia depends heavily on the mass eccentricity between the cross section center of gravity and the local center of gravity of the twin boxes. Important cross section structural properties of the elements used in the model are given in Table 1, while different deck configurations are presented in Table 2. In the present case study, it was assumed that the cross beams between the twin boxes were infinitely stiff and their mass was neglected.

Table 1. Cross section structural properties in the finite element model

	Cross section structural properties					
	E $[GPa]$	I_y $[m^4/m]$	I_z $[m^4/m]$	I_v $[m^4/m]$	m $[t/m]$	A m^2
Main cable	205	-	-	-	13.164	1.54
Hangers	180	-	-	-	0.05	0.005
Pylon legs	210	334	118	325	68.923	8.78
Pylon bracings	210	115	42	98	24.311	3.10

It is evident that the key to decrease γ_ω, is to decrease the cable eccentricity e_k compared to the mass eccentricity e_m. A twin bridge design, with the bridge deck placed external to the cable planes, as illustrated in Figure 3, allows this construction (Bartoli et al., 2008; Richardson, 1981).

Several models have been evaluated for their frequency ratios between vertical and torsional modes, of which three is presented in Table 2.

Table 2. Bridge deck cross section structural properties for three of bridge deck configurations

	Bridge deck cross section structural properties									
Deck	γ_ω -	e_m $[m]$	e_k $[m]$	m $[t/m]$	I $[t \cdot m^2/m]$	E $[GPa]$	G $[GPa]$	I_y $[m^4/m]$	I_z $[m^4/m]$	I_v $[m^4/m]$
(a)	1.4	11.5	5	14.57	3101	210	81	7.27	147.74	2.08
(b)	0.89	20	10	14.57	7002	210	81	7.27	412.81	2.08
(c)	0.92	40	30	14.57	24488	210	81	7.27	1600.81	2.08

On the basis of these, it has been feasible to invert the natural frequencies with the following parameters: $e_k = 10$ m and $e_m = 20$ m, ie. bridge deck (b) in Table 2. The still air modal analysis of bridge deck (b) is presented in Section 3.1. Bi-modal coupling analysis of the vertical and torsional mode shapes and their respective frequency ratios of this model are presented in Section 3.2 while a multimodal analysis is presented in Section 3.3.

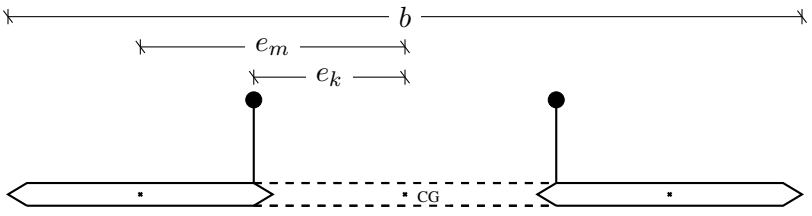

Figure 3. Cross section design principle

3.1 Global modal analysis

Prior to the modal analysis, the static force equilibrium equations were solved and the stiffness effects of deflection and internal forces due to dead load of the bridge was taken into account.The eigenvalue problem of the mass- and stiffness matrices were solved using block Lanczos algorithm.

The results of the global modal analysis for the first 20 modes are listed in Table 3, which fairly illustrate the incidence of the mode shape variations. Each mode shape is plotted along the bridge deck axis in the vertical and the horizontal plane.

Table 3. Modal analysis. The natural modes are listed according to their natural frequency ω in ascending order and their mode shapes are plotted and described where S: Symmetric. A:Anti-symmetric. L: Lateral. V: Vertical. T:Torsional.

Modal analysis					
ID	ω $[Rad/s]$	f $[Hz]$	Description	Vertical plane	Horizontal plane
1	0.194	0.031	1SLT		
2	0.328	0.052	1AT		
3	0.369	0.059	1AV	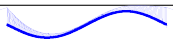	
4	0.407	0.065	1ALT		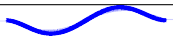
5	0.412	0.066	1ST		
6	0.463	0.074	Cables		
7	0.484	0.077	1SV		
8	0.519	0.083	Cables		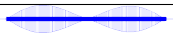
9	0.542	0.086	2ST		
10	0.591	0.094	2ALT		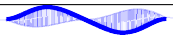
11	0.603	0.096	LT + Pylons + Cables		
12	0.647	0.103	2SV		
13	0.651	0.104	2AT		
14	0.672	0.107	2SLT		
15	0.724	0.115	2AV		
16	0.797	0.127	Cables		
17	0.819	0.130	3ST		
18	0.86	0.137	LT + Pylons + Cables		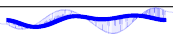
19	0.917	0.146	LT + Pylons + Cables		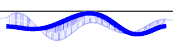
20	0.919	0.146	3SV	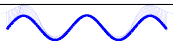	

3.2 Bi-modal coupling coefficients

Selected results of the modal analysis are presented in Table 4 for the first five torsional and vertical mode shapes. The ID refers to Table 3, while α_m and ξ_n is the pitching and heaving mode where m and n is the number of half waves.

The natural frequency of the vertical mode shapes are higher than the corresponding torsional mode shapes, which is opposite traditional bridge design, ie. long span suspension bridges in service today.

Only mode shapes with dominating vertical displacements or torsional rotation has been selected. Lateral-torsional-bending mode shapes of the bridge deck, were observed in the modal analysis, but not included in the present bi-modal mode coupling analysis. The influence of these modes are considered in the multimodal analysis in Section 3.3.

Table 4. The five lowest pure torsional and vertical mode shapes of the bridge deck

Torsional mode shapes (a)				Vertical mode shapes (b)			
ID	α_m	ω_{α_m}	Mode shape	ID	ξ_n	ω_{ξ_n}	Mode shape
2	α_2	0.328		3	ξ_2	0.369	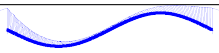
5	α_1	0.412		7	ξ_1	0.484	
9	α_3	0.542		12	ξ_3	0.647	
13	α_4	0.651		15	ξ_4	0.724	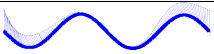
17	α_5	0.819		20	ξ_5	0.919	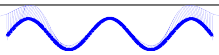

Table 5. Frequency ratios and mode shape coupling constants

Torsional-to-vertical frequency ratios (a) $\gamma_\omega = \frac{\omega_{\alpha_m}}{\omega_{\xi_n}}$						Mode shape coupling constants (b) $c_{\xi_n} c_{\alpha_m}$					
	ξ_2	ξ_1	ξ_3	ξ_4	ξ_5		ξ_2	ξ_1	ξ_3	ξ_4	ξ_5
α_2	**0.88**	0.68	0.51	0.45	0.36	α_2	**1**	0	0	0	0
α_1	1.11	**0.9**	0.64	0.57	0.45	α_1	0	**0.96**	0.05	0	0
α_3	1.47	1.12	**0.89**	0.75	0.59	α_3	0	0.04	**0.95**	0	0
α_4	1.76	1.34	1.01	**0.85**	0.71	α_4	0	0	0	**1**	0
α_5	2.22	1.69	1.27	1.13	**0.84**	α_5	0	0	0	0	**1**

From Table 4 and 5 it is seen that if the torsional-to-vertical frequency $\gamma_\omega > 1$, the mode shape coupling constants $c_{\xi_n} c_{\alpha_m} = 0$, except for the second torsional symmetric mode α_3 combined with the first vertical symmetric mode ξ_1, which has a mode shape coupling constant $c_{\xi_1} c_{\alpha_3} = 0.04$ and a torsional-to-vertical frequency ratio $\gamma_\omega = 1.12$. The root curves of the flutter determinant for this bi-modal combination is plotted in Figure 5 (b).

The numerical results of the case study verifies the theoretical analysis in Section 2.

3.3 Multimodal flutter analysis

The multimodal flutter approach developed by (Jain et al., 1996) has been implemented for the first 20 modes in order to estimate flutter instabilities of bridge model (b) presented in Section 3, Table 2.

The bridge deck flutter derivatives $A_1^*(K)$-$A_4^*(K)$ and $H_1^*(K)$-$H_4^*(K)$ where the non-dimensional frequency, $K = \frac{b\omega}{U}$ where ω is the circular frequency of the oscillation of the bridge deck at the wind velocity, U, are replaced with those of a thin airfoil and follows Dyrbye and Hansen (1997, page 151). The thin airfoil approximation of the bridge deck is an extreme assumption. The shape of the bridge deck in the case study is actually unknown, which complicate the choice of valid flutter derivatives. The lateral bridge deck flutter derivatives $P_1^*(K)$-$P_6^*(K)$, $A_5^*(K)$-$A_6^*(K)$ and $H_5^*(K)$-$H_6^*(K)$ are calculated according to quasi-steady theory, where the static drag, lift and moment coefficients are $c_d = 0.32$, $c_l = 0.0942$ and $c_m = 0.0104$ respectively. The slope of the lift curve at $\alpha = 0$ are considered flat, ie. $dc_d/d\alpha = 0$ (Chen et al., 2000).

The critical flutter wind velocity, U_{cr} is identified at the intersection point between a real and an imaginary root curve. Figure 4 plots real and imaginary root curves for the first 20 modes of bridge deck model (b), where the bridge deck width, $b = 60$ m. The areas highlighted in red on the plots corresponds to wind velocities $U \leq 100m/s$. The root curves of mode 1, 2 and 3 becomes very close at low non-dimensional frequencies, but no intersection occurs for values of $0.02 \leq K$. The lowest frequency at $K = 0.02$ is $\omega = 0.02611rad/s$ for the imaginary part of the root curve of mode 2, which corresponds to a full scale wind velocity $U = \frac{b\omega}{K} = 78.3m/s$.

At a very high wind velocity, however, coupled flutter with participation of the second symmetric torsional mode and an antisymmetric lateral mode, appear. The still air mode shapes corresponds to mode 9 and 10, given in Table 3. The nature of this particular flutter instability mechanism is very rare. The intersection point between the root curves of mode 9 and 10 is found at $K = 0.025$ and $\omega = 0.46$ rad/s in Figure 4 (b), corresponding to a critical flutter wind velocity $U_{cr} = \frac{b\omega}{K} = 1104m/s$, which is obviously beyond the scope of aerodynamic design of civil engineering structures.

3.4 Bi-modal flutter analysis

Considering the motion-induced wind load for the first antisymmetric modes α_2 and ξ_2 only, reveals that torsional flutter occur at a critical flutter wind velocity $U_{cr} = 56.7m/s$, in bridge model (a), where the bridge deck width is $b = 26m$. For bridge model (b), no flutter instabilities were found between any bi-modal combinations of the first 20 modes. Figure 5 plots the root curves of α_2 and ξ_2 for bridge model (a) and (b) respectively.

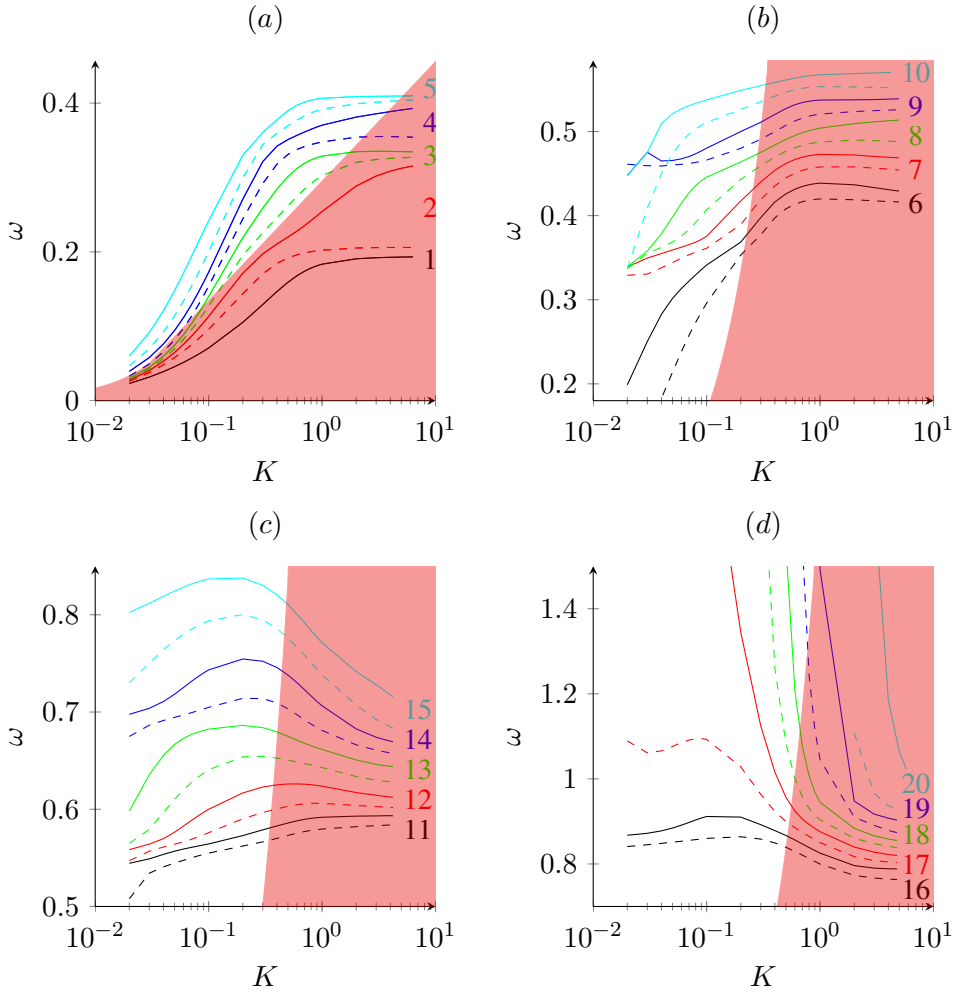

Figure 4. Multimodal flutter root curves of bridge model (b) presented in Section 3, Table 2. The cyclic frequency of oscillation ω in rad/s is plotted against the reduced frequency $K = \frac{b\omega}{U}$. Mode 1 to 5 is plotted in sub plot (a), mode 6 to 10 in sub plot (b), mode 11 to 15 in sub plot (c) and mode 16 to 20 is plotted in sub plot (d).

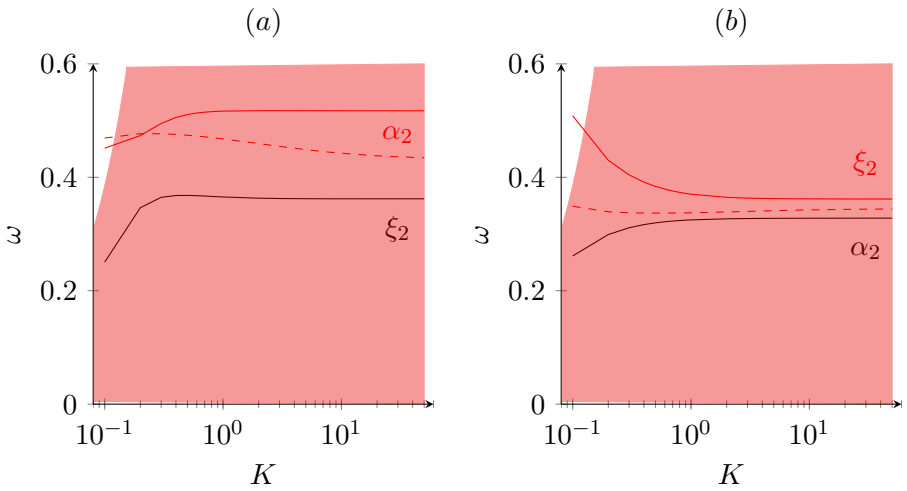

Figure 5. Bi-modal flutter root curves of the first antisymmetric vertical (α_2) and antisymmetric torsional (ξ_2) modes of bridge model (a) and (b) presented in section 3 Table 2, with bridge deck width $b = 26m$. Flutter occur in model (a) at $(K, \omega) = (0.22, 0.48)$ resulting in a critical flutter wind velocity $U_{cr} = 56.7m/s$.

4 Conclusion

It is possible to design a suspension bridge with a torsional-to-vertical frequency ratio below 1. Bimodal coupled flutter between higher torsional modes with lower vertical modes, where their respective torsional-to-vertical frequency ratio will be above 1, is avoided, because the mode shape coupling constants is zero or at least very close to zero.

A multimodal flutter analysis, considering the first 20 modes, revealed solely flutter mechanisms at very high wind velocities. The lowest flutter velocity was $U_{cr} = 1104$ m/s. for a lateral-torsional mode coupled with the second symmetric torsional mode.

Further studies are needed to clarify the influence of $\gamma_\omega \leq 1.1$ on twin bridges and the implementation of real bridge deck flutter derivatives in a multimodal flutter analysis of a suspension bridge.

5 Acknowledgments

Jens Johansson[1], Michele Starch Øvre[1], Svend Ole Hansen[1&2], Allan Larsen[3], Martin Nymann Svendsen[4] and Simon Rex[4] are gratefully acknowledged for their inputs during our work with the non-flutter design principle. [1]University of Southern Denmark. [2]Svend Ole Hansen Aps. [3]COWI. [4]Ramboll.

6 References

References

Bartoli, G., D'Asdia, P., Febo, S., Mannini, C., Noe, S., and Procino, L. (2009). Innovative configurations for long-span suspension bridges. *Proceedings of the 5th European and African Conference on Wind Engineering*. Florence, Italy.

Bartoli, Gianni, D'Asdia, Piero, Febo, Sofia, Mannini, Claudio, Past, Stefano, and Procino, Lorenzo (2008). Innovative Solutions for long-span suspension bridges. *BBAA VI International Colloquium on: Bluff Bodies Aerodynamics Applications*.

Bleich, Freidrich, McCullough, C. B., Rosecrans, Richard, and Vincent, George S. (1950). *The mathematical theory of vibration in suspension bridges*. Department of commerce bureau of public roads.

Chen, Xinzhong, Matsumoto, Masaru, and Kareem, Ahsan (2000). Aerodynamic Coupling Effects on Flutter and Buffeting of Bridges. *Journal of Engineering Mechanics* **126**, pp. 17–26.

Dyrbye, Claus and Hansen, Svend Ole (1997). *Wind loads on Structures*. Wiley.

Gimsing, N. J. and Georgakis, C. T. (2012). *Cable Supported Bridges*. Third edition. Wiley.

Jain, A., Jones, N., and Scanlan, R. (1996). Coupled Flutter and Buffeting Analysis of Long-Span Bridges. *Journal of Structural Engineering* **122**, pp. 716–725.

Johansson, J., Andersen, M.S., and Øvre, M.S. (2013). Non-flutter design principle for long span bridges. *Proceedings of the Eighth Asia-Pacific Conference on Wind Engineering*.

Nowicki, T. and Flaga, A. (2011). Relation between shape and the phenomenon of flutter for bridge deck-like bluff bodies. *Archives of Mechanics* **63**.2, pp. 201 –220.

Richardson, J. R. (1981). The development of the concept of the twin suspension bridge. *NMI R125*.

Theodorsen, T. (1934). General theory of aerodynamic instability and the mechanism of flutter. *NACA Report* **496**, pp. 291–311.